STUDIA UBB CHEMIA, LXXI, 2, 2026 (p. 307-334)
(RECOMMENDED CITATION)
DOI:10.24193/subbchem.2026.2.16

PLA - ZnO COMPOSITE WITH BACTERICIDAL AND FUNGICIDAL ACTIVITY

Raluca-Elena DRAGOMIR[a], Cristina-Maria DUȘESCU-VASILE[a], Andra-Ioana STĂNICĂ[b], Marian BĂJAN[a], Daniel BOMBOȘ[c], Ioan SAROSI[d], Andrei MOLDOVAN[d], Gabriel VASILIEVICI[e*]

ABSTRACT. A plasticized polylactic acid (PLA) composite incorporating zinc oxide (ZnO) was synthesized via melt mixing and hot pressing. The physicochemical and preliminary microbiological properties of the composite were systematically evaluated. ZnO powder, produced through precipitation and calcination, was characterized using dynamic light scattering and nitrogen sorption analysis. The PLA composite, comprising PLA, Proviplast 2624, Span 60, and ZnO, was subjected to tensile and flexural testing, oxygen and water vapor barrier measurements, water uptake analysis, contact angle assessment, and Atenuated Total Reflectance – Fourier Transform Infrared spectroscopy (ATR-FTIR). The ZnO powder exhibited a broad, aggregate-dominated particle-size distribution and a moderate specific surface area. The composite displayed reduced stiffness and strength relative to neat PLA, indicating effective plasticization. Preliminary microbiological assays indicated decreased recovery of the tested microorganisms under the specified conditions.

Keywords: *PLA composite, Proviplast 2624, ZnO, Bacillus subtilis, Aspergillus mold*

[a] *Department of Petroleum Refining Engineering and Environmental Protection, Petroleum-Gas University of Ploiesti, 39 Bucharest Blvd., 100680 Ploiesti, Romania.*
[b] *Technological Highschool "Toma Socolescu", Gheorghe Grigore Cantacuzino St., 328, 100466 Ploiești, Romania.*
[c] *S.C. Medacril S.R.L, 8 Carpați Street, Mediaş, Sibiu County, Romania.*
[d] *Department Environmental Engineering and Sustainable Development Entrepreneurship, Technical University of Cluj-Napoca, 400641 Cluj-Napoca, Romania.*
[e] *National Institute for Research Development for Chemistry and Petrochemistry-ICECHIM-București, 202 Spl. Independenței, 060021, Bucharest, Romania.*
[*] *Corresponding author : gvasilievici@icechim.ro*

INTRODUCTION

The most widely used thermoplastics globally are polyethylene (PE) and polypropylene (PP) but they share a common challenge: because they degrade slowly, they contribute to long-term ecological damage [1]. The degradable alternatives are (bio)polymers such as PBS (polybutylene succinate) and PLA obtained from renewable resources such as corn starch and sugarcane [2-3] and poly(hydroxyalkanote)s (PHAs) produced by bacterial fermentation. Yu et al. have investigated the potential antimicrobial ZnO's properties through the PLA integration. Their results demonstrated improved degradability, antibacterial activity and enhanced air filtration performance, framing PLA/P(3HB-co-4HB)/ZnO melt-blown nonwovens as well-suited options for next-generation sustainable air filters, medical masks, and protective healthcare textiles. PLA has also garnered considerable attention from food packaging industry experts due to its high transparency, good biological compatibility and high tensile plasticity. Considerable scientific inquiry has concentrated on adapting PLA structure to enhance its functional performance and increase its versatility. Li et al. obtained an electrospun PLA composite by incorporating different concentrations of ZnO nanoparticles and evaluated their mechanical, thermal, hydrophobic, and antibacterial properties. Moreover, they studied the effectiveness of these materials in preserving fresh chicken meat, establishing a foundation for degradable antibacterial food packaging [4].

Torche et al. have recently explored the alternative of using deep eutectic solvents (DESs) obtained by complexation between hydrogen-bond donors and quaternary ammonium salts. The obtained PLA-based composite plasticized with DESs and reinforced with green-synthesized ZnO particles derived from date palm seed extracts exhibited robust antibacterial efficacy, most notably at a 3 wt% ZnO concentration, demonstrating substantial reductions in *Staphylococcus aureus* and *Escherichia coli*, alongside complete inhibition of the spore-forming pathogen *Bacillus cereus* [5].

Significantly valued since the days of antiquity for its extensive economic importance and medicinal properties, *mesquite* or *algarroba*, belonging to the *Prosopis* family, continues to be utilized globally. Scientific research reveals that pastes, gums, and leaf smoke derived from the plant contain bioactive compounds that fight cancer, diabetes, inflammation, and microbial infections. Raja Thandavamoorthy et al. aimed to select the optimal materials for developing a composite made of epoxy resin matrix reinforced with *Prosopis juliflora* fibers (PJFR) and zinc oxide particles, to be fabricated via the conventional hand layup method. They evaluated the mechanical, thermal, and morphological characteristics of an innovative PJ composite,

showing that the addition of zinc oxide as a filler material significantly enhanced the thermal performance of the PJ fiber composite, yielding an average improvement of 26.7% [6].

A novel approach was introduced by Chen et al. by using 3-aminopropyltriethoxysilane (APTES) to form capped ZnO quantum dots. The study investigates the structure–property relationships of AC-ZnQDs/PLA composites, highlighting that the end-group modulation fundamentally transforms polymer performance by tailoring chain-end chemistry. This targeted structural tuning drives simultaneous optimization across three critical areas: interfacial compatibility, mechanical integrity and hydrolytic degradation [7].

Detecting microorganisms contaminating membrane surfaces is essential across fields such as biotechnology, environmental engineering, the food industry, pharmaceuticals, and medical applications. Membrane surfaces are used in separation processes, coarse particle filtration, and biological treatment plants to purify water containing persistent pollutants [8-13]. Microbial colonization of these surfaces can cause biofouling, structural degradation, and reduced performance.

Membrane surfaces serve as effective substrates for microorganisms, including bacteria, fungi, and microalgae. Once attached, these organisms may form biofilms, complex communities embedded in a polymeric extracellular matrix. Biofilm formation reduces membrane permeability, increases hydraulic resistance, and impacts separation selectivity. Microbiological testing identifies colonizing species and assesses their ability to adhere to and grow on membrane surfaces [14].

Assessing microorganisms is crucial for ensuring the safety and stability of membrane-based systems. In medical and pharmaceutical settings, microbiological contamination can compromise product or equipment sterility and pose serious health risks. In water treatment, ultrafiltration, and microfiltration, microbial communities on membranes can decrease purification efficiency and contaminate the final product. Studying how microorganisms interact with membrane surfaces helps identify surface properties, such as roughness, hydrophobicity, electrical charge, and chemical composition, that influence microbial adhesion. These insights guide the development of antimicrobial membranes, which can extend the operational lifespan of filtration systems [15].

Microbiological testing guides the development of effective strategies for preventing and controlling contamination. Identifying dominant microbial species and their adhesion and proliferation mechanisms enables the selection of appropriate cleaning, disinfection, or sterilization procedures for membranes. Microbiological monitoring is therefore essential for operational

management in membrane-based systems. Testing for microorganisms that can contaminate membrane surfaces helps clarify colonization mechanisms, maintain membrane performance, and ensure process safety [16-20]. This approach also helps prevent premature material degradation and supports the development of new technologies to reduce microbiological contamination.

The goal of our study is to help design versatile, environmentally friendly PLA materials with high bactericidal activity that are both sustainable and biodegradable.

RESULTS AND DISCUSSION

Characterization of ZnO powder

Determination of particle size distribution. For this study, 0.03 g of the sample was dispersed in 25 mL of distilled water. Further, the resulting dispersion was ultrasonicated in a water bath for approximately 3 minutes to separate aggregated particles. The results of Dynamic Light Scattering (DLS) are presented in Table 1 and Figures 1 and 2.

Table 1. Evaluation of particle size by DLS

Sample	Dm (nm)	PdI	Peak position by intensity (nm)
ZnO	840± 56	0.697	P_1 = 873 P_2 = 216

The relatively high average hydrodynamic particle size (Dm) can be attributed to the elevated NaOH dosing flow rate of 0.5 mL/min, which results in less controlled nucleation and the formation of larger particles. A 30-minute post-reaction at 60°C can facilitate the dissolution of smaller particles and the growth of larger ones, thereby narrowing the size distribution and increasing the average size. Calcination at 300°C for 4 hours, with a heating rate of 10°C/min, achieves complete conversion of $Zn(OH)_2$ to ZnO and promotes moderate particle growth via incipient sintering. Ethanol washing decreases particle agglomeration, although it does not entirely prevent it.

The Polydispersity Index (PdI) highlights the inhomogeneity of the particle population size. Thus, the polydispersity index value of 0.697 suggests a multimodal population distribution. Also, the relatively high PDI value indicates that particle populations with very different sizes coexist, the nucleation process was uncontrolled, and there are probably agglomerates alongside primary particles.

Figure 1 shows a bimodal particle size distribution, with populations averaging 873 nm and 216 nm, as the average of five determinations. Larger aggregates are also present, as indicated by the correlation curve in Figure 2.

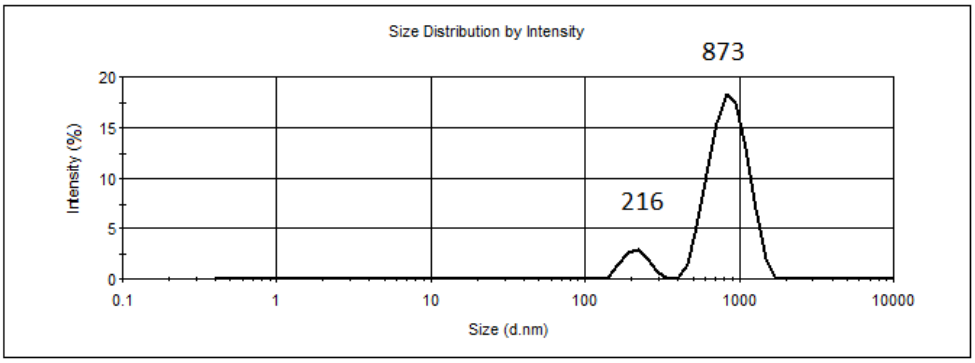

Figure 1. Size distribution for ZnO powder

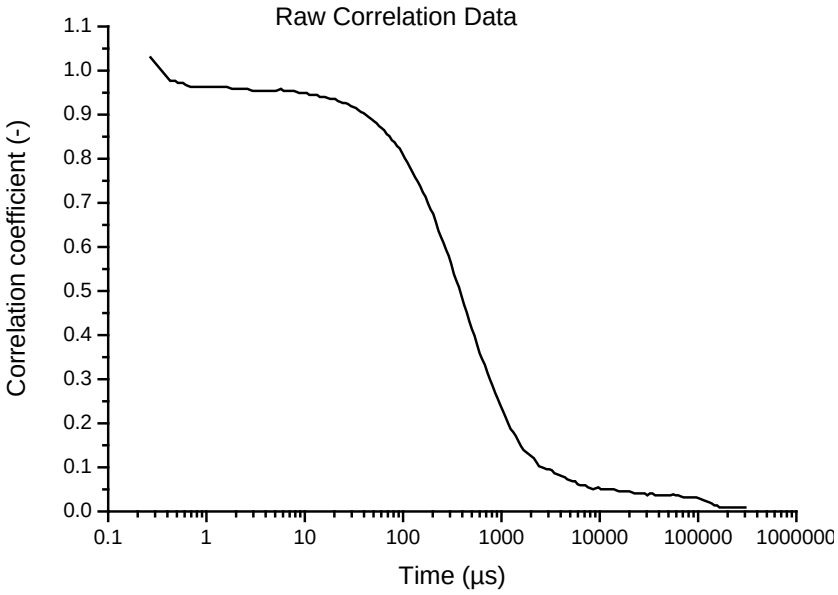

Figure 2. Correlation curve

Determination of textural characteristics. The specific surface area, total pore volume, and average pore diameter were determined by nitrogen adsorption (Figures 3-4, Table 2).

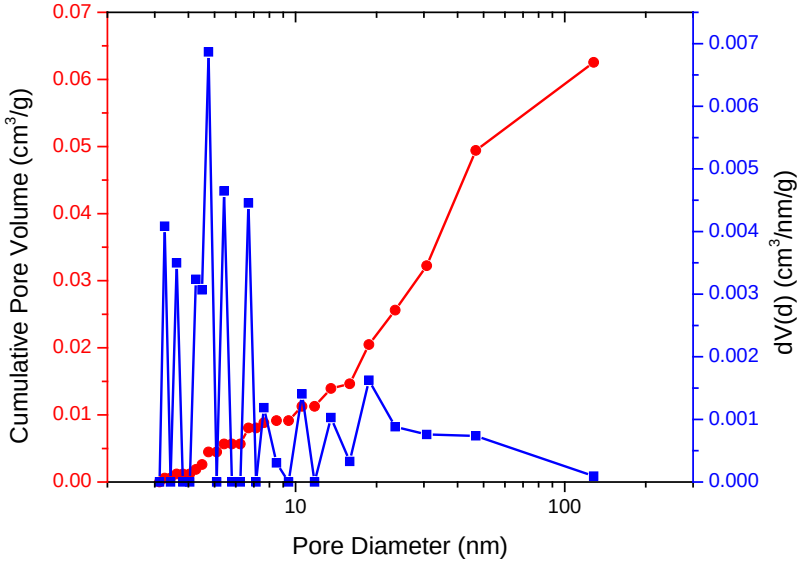

Figure 3. The pore size distribution of ZnO powder

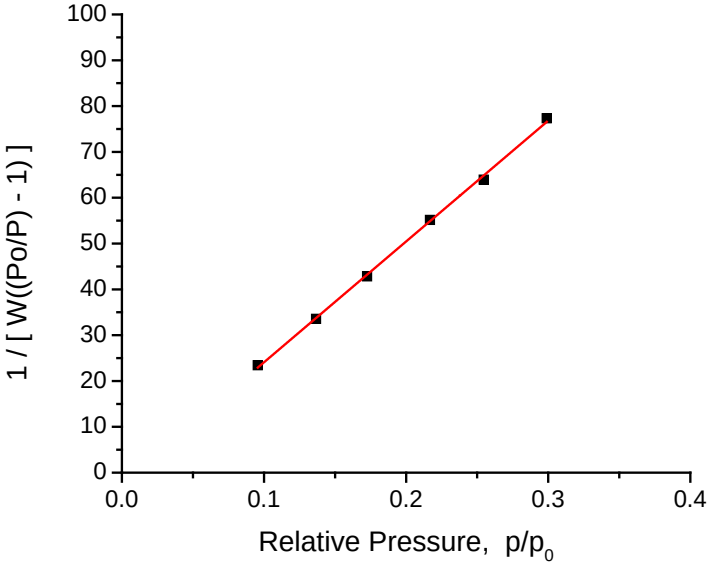

Figure 4. Multi-Point BET (Brunauer–Emmett–Teller) Plot

Table 2. Textural characteristics of ZnO powder particles

Sample	Specific surface area (m^2/g)	Total pore volume (cm^3/g)	Mean pore diameter (nm)
ZnO	13.744	0.063	4.750

The BET-specific surface area is relatively low for ZnO powder, indicating particles that are small-sized but partially agglomerated or sintered. Thus, the specific surface area indicates the formation of ZnO particles in the submicron range, but also significant agglomeration after calcination at 300°C. Therefore, the value of 13.7 m^2/g indicates a reduction in surface area due to a slight sintering during calcination.

The total pore volume indicates low to moderate porosity, reflecting interparticle spaces and pores formed upon removal of water and hydroxide. The relatively low total pore volume suggests particle compaction or aggregation and possible densification during heat treatment. This value demonstrates the existence of accessible, predominantly interparticle porosity. In systems produced by NaOH precipitation, gel or hydroxide drying, and calcination, pores typically form through water removal, decomposition of $Zn(OH)_2$ or basic intermediates, and aggregate reorganization.

The average pore diameter falls within the mesoporous range (2–50 nm, as defined by IUPAC), indicating a relatively uniform structure with free spaces between nanoparticles or aggregates. Such porosity is advantageous for antimicrobial activity and promotes effective dispersion in polymer matrices, such as PLA.

From the multipoint BET graph (Figure 4), it can be seen that the points are well aligned, confirming good linearity of the experimental values in the analyzed relative pressure range, with a correlation coefficient very close to 1. Thus, the BET specific surface area, obtained from automatic sample processing, indicates a relatively moderate value, consistent with an oxide with relatively agglomerated or partially sintered particles.

SEM analysis of ZnO powder. Scanning electron microscopy (SEM) analysis of ZnO powder at a 4 μm scale (Figure 5) reveals that the smallest visually distinguishable particles measure approximately 80–150 nm. Significant agglomeration obscures individual particle boundaries, resulting in poorly defined edges. The SEM image predominantly displays micrometric aggregates composed of smaller primary particles, with the smallest visible formations estimated at 50–150 nm.

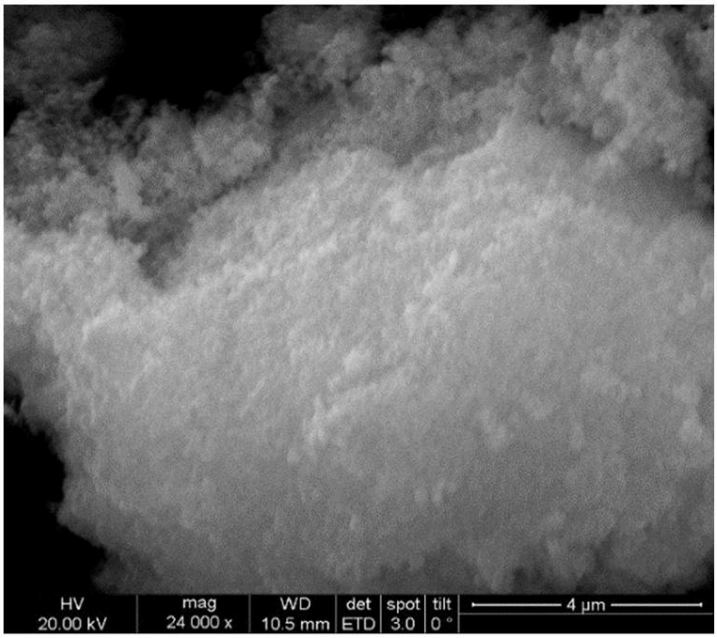

Figure 5. SEM image of ZnO

The SEM image supports the results obtained from DLS analysis, indicating that ZnO particles are strongly agglomerated and do not appear as well-separated individual particles.

In summary, the SEM image of ZnO powder demonstrates an agglomerated morphology, with fine particles forming irregular micrometric aggregates. This observation indicates substantial agglomeration of primary particles into larger clusters. The non-uniform size distribution and observed surface roughness suggest the presence of interparticle spaces, which may contribute to porosity, as confirmed by BET analysis.

Mechanical Properties of the ZnO-reinforced PLA composite

Bending test interpretation. The mechanical performance of the ZnO-reinforced PLA composite, plasticized with Proviplast 2624 and Span 60, reveals a significant behavior change compared to pure PLA. Thus, as shown in Tables 3 and 4, the material's mechanical behavior changes radically, especially at low temperatures (4°C and -18°C). Normally, pure PLA (from Ingeo) is a rigid and brittle polymer, especially at temperatures below its glass transition temperature (approx. 55−60ºC). Both at 4ºC and especially at -18ºC, pure PLA becomes extremely brittle, with a very high Young's Modulus (often between 2000 and 3500 MPa) and a very low elongation at break.

Although ZnO acts as a stiffener and nucleating agent, in the presence of a large amount of plasticizers such as Proviplast 2624 and Span 60 (17% in total), the flexibilization effect of the plasticizers dominates the matrix, increasing the free volume and molecular mobility. This dramatically decreases the Young's Modulus (stiffness) and increases flexibility, even at freezing temperatures. Thus, the Young's Modulus (approx. 437 MPa) is very low compared to pure PLA (which at 4ºC is over 3000 MPa). This demonstrates the efficiency of the Proviplast 2624 plasticizer, the composite becoming extremely flexible and elastic at a temperature close to that of a food refrigerator. Also, the maximum bending stress (approx. 28 MPa) is lower than in pure PLA (which can exceed 60-80 MPa).

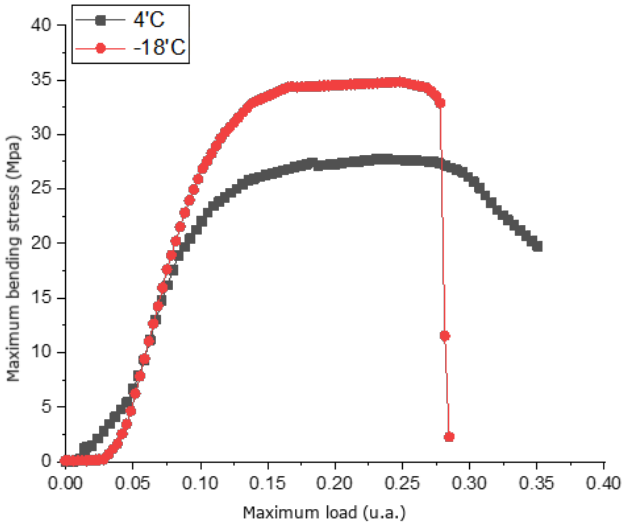

Figure 6. Variation of maximum bending stress with load, at 4ºC and -18ºC

The material yields at much lower forces because plasticization has reduced the polymer's internal cohesion. Although the material is flexible (low modulus), the capacity for plastic deformation at this temperature, as evidenced by the elongation value, remains relatively limited before a crack initiates. Normally, as the temperature decreases from 4ºC to -18ºC, polymers become stiffer and more brittle. Thus, an increase in the Young's modulus (to 517 MPa) and the maximum bending stress at maximum load (35 MPa) is normal. At -18ºC, the movement of the PLA and plasticizer chain segments is further reduced, making the material stiffer and capable of supporting a higher maximum load (83 N versus 63 N). The fact that the elongation increased by more than 3 times suggests a synergistic toughening

mechanism at extremely low temperatures, probably due to controlled phase separation. Thus, at -18ºC, Proviplast 2624 or Span 60 could form distinct micro-domains that deflect microcracks and allow the composite to deform further before complete failure. Therefore, Figure 6 highlights the superior behavior of the sample at -18ºC, as evidenced by the maximum load supported, stiffness, and maximum bending stress.

Table 3. Results obtained from the bending test at 4ºC

Maximum load (N)	**Young's modulus** in bending **(MPa)**	Bending stiffness **(Nm²)**	Maximum bending stress at maximum load **(MPa)**	Elongation **(mm)**
63.194 ± 2.13	436.667 ± 9.14	0.011 ± 0.002	27.750± 0.95	1.265± 0.23

Table 4. Results obtained from the bending test at a temperature of -18ºC

Maximum load (N)	Young's modulus in bending **(MPa)**	Bending stiffness **(Nm²)**	Maximum bending stress at maximum load **(MPa)**	Elongation **(mm)**
83.000 ± 2.61	517.094 ± 11.25	0.014± 0.003	34.824± 1.28	4.054± 0.71

Table 5 presents the tensile test results, and Figure 7 shows the tensile deformation curve.

Table 5. Results obtained from the tensile test

Tensile strength (MPa)	**Maximum load (N)**	**Breaking load (N)**	**Elongation at break (mm)**	**Young's modulus (MPa)**	**Tensile strength at break (MPa)**
13.650± 0.72	143.609 ± 3.97	142.628± 3.47	5.246± 0.82	512.298 ± 10.41	13.557 ± 0.63

Flexural Properties. The flexural properties of the ZnO-reinforced PLA composite plasticized with Proviplast 2624 and Span 60 are presented in Tables 3 and 4. The results indicate that storage temperature significantly influenced the mechanical response of the material. At 4 ºC, the composite exhibited a flexural modulus of 436.67 MPa, a maximum bending stress of 27.75 MPa, and a maximum load of 63.19 N. After storage at −18 ºC, these values increased to 517.09 MPa, 34.82 MPa, and 83.00 N, respectively.

The increase in flexural modulus and maximum bending stress at −18 ºC indicates a stiffer and stronger material under bending conditions. This behavior is consistent with the reduced mobility of polymer chains at lower temperatures, which generally leads to increased rigidity. Despite the presence of ZnO, which may contribute to reinforcement of the PLA matrix, the relatively low modulus values compared with those typically reported for neat PLA suggest that the plasticizing effect of Proviplast 2624 and Span 60 plays a dominant role in determining the overall mechanical behaviour of the composite.

The elongation value increased from 1.27 mm at 4 ºC to 4.05 mm at −18 ºC. Although this result suggests an improved deformation capacity before failure, additional microstructural investigations would be required to identify the mechanisms responsible for this behaviour. Overall, the composite maintained its structural integrity at both storage temperatures while exhibiting higher stiffness and load-bearing capacity at −18 ºC.

Tensile Properties. The tensile properties of the ZnO-reinforced PLA composite are presented in Table 5. The material exhibited a tensile strength of 13.65 MPa, a maximum load of 143.61 N, a breaking load of 142.63 N, and a Young's modulus of 512.30 MPa. The small difference between the maximum load and breaking load indicates that failure occurred shortly after the maximum stress was reached.

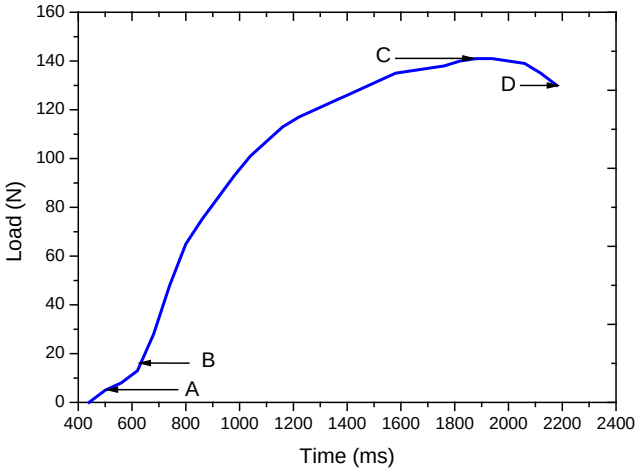

Figure 7. Tensile strain curve of PLA-ZnO composite

The measured Young's modulus was substantially lower than values commonly reported for neat PLA, confirming the effectiveness of the plasticizers in reducing matrix stiffness. The elongation at break of 5.25 mm indicates a moderate capacity for deformation before failure. These results

demonstrate that incorporating Proviplast 2624 and Span 60 modifies the mechanical response of PLA, producing a material with reduced stiffness and moderate flexibility while maintaining sufficient mechanical strength for handling and packaging applications.

Overall, the combination of ZnO and plasticizers resulted in a composite characterized by lower rigidity than conventional PLA and satisfactory mechanical performance over the investigated temperature range.

SEM analysis of the ZnO-reinforced PLA composite. The SEM image demonstrates that the PLA ZnO composite exhibits a uniform morphology. The polymer displays a homogeneous microstructure without evidence of phase separation (Figure 8). Furthermore, the incorporation of ZnO particles into PLA does not alter the composite surface, resulting in a smooth, non-porous foil that does not promote biological activity such as adhesion, migration, or proliferation of cultured cells.

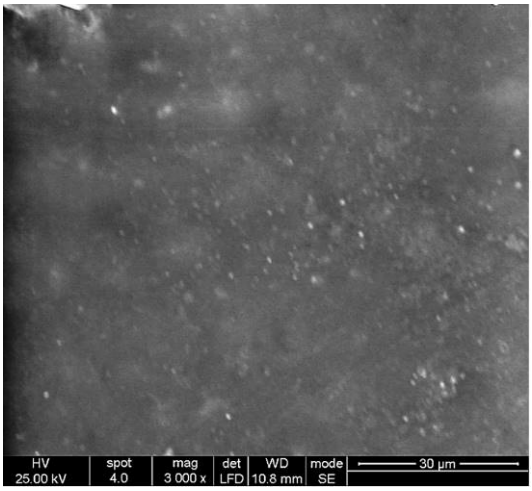

Figure 8. SEM micrograph of the ZnO-reinforced PLA composite

The SEM micrograph (Figure 8) reveals a relatively homogeneous and continuous surface morphology of the ZnO-reinforced PLA composite. Numerous fine bright spots are distributed throughout the polymer matrix that can be attributed to ZnO particles dispersed within the PLA. Although small-localized agglomerates are visible, no large clusters, cracks, or significant voids were observed, indicating a satisfactory distribution of the inorganic phase in the plasticized PLA matrix.

The absence of major structural defects suggests adequate compatibility between the matrix and the filler, which may contribute to the overall mechanical integrity of the PLA composite. The relatively uniform morphology is consistent with the mechanical results, where the material exhibited sufficient strength while maintaining moderate flexibility due to the plasticizing effect of Proviplast 2624 Span 60.

Barrier properties of the ZnO-reinforced PLA composite

Determination of oxygen permeability. Permeability was measured at 1 atm pressure, temperature 23ºC, and 0% relative humidity for 5 specimens of PLA composite containing ZnO. Table 6 presents the thickness and the average oxygen permeability and normalized oxygen permeability values of the PLA-ZnO composite, both normalized to a layer thickness of 1 mm.

Table 6. Oxygen Permeability Test (OTR) Results

Sample	Sample thickness (mm)	OTR, (mL/m^2 x day)	OTR, $mL/m^2 \cdot day$ (relative to a thickness of 1 mm)
PLA-ZnO	0.97	106.53± 0.83	109.82± 0.86

Table 6 indicates that the tested PLA formulation exhibits more than five times higher oxygen permeability compared to pure PLA [21]. This increase is attributed to relaxation of the polymer structure and enhanced PLA chain mobility resulting from the high concentration (15% wt.) of Proviplast 2624 plasticizer. The barrier effect of ZnO is substantially diminished due to this increased chain mobility. Furthermore, Span 60 acts as an interfacial lubricant, thereby facilitating oxygen diffusion through the PLA membrane.

Oxygen permeability in the PLA formulation is mainly determined by the plasticizer content and polarity, rather than by the powder content. The addition of non-polar plasticizers increases the formulation's oxygen permeability. When the polarity of the plasticizer matches that of the polymer, swelling increases free volume and oxygen permeability. Materials that block pores can partially offset this increase in oxygen diffusion. Consequently, adjusting the concentration of inorganic powders enables control over oxygen permeability in PLA-based composites, even when high levels of polar plasticizers such as Proviplast 2624 are present.

Water absorption. Figure 9 presents the results obtained. The absorption rate at both temperatures is initially higher, as indicated by the steeper slope of the curve, and subsequently decreases, approaching

equilibrium (saturation) around days 6 to 7. On day 7, both samples reach an identical absorption value of 0.47%. This finding suggests that the maximum absorption capacity of the polymer network in 10% saline solution is determined by the chemical structure of PLA and the presence of salt, rather than by temperature. The higher initial diffusion rate observed at elevated temperature is attributed to increased kinetic energy of water molecules and greater mobility of the polymer chains. At 23ºC, the free volume between PLA chains forms and changes more rapidly, enabling the saline solution to penetrate the matrix more efficiently during the initial phase of the experiment.

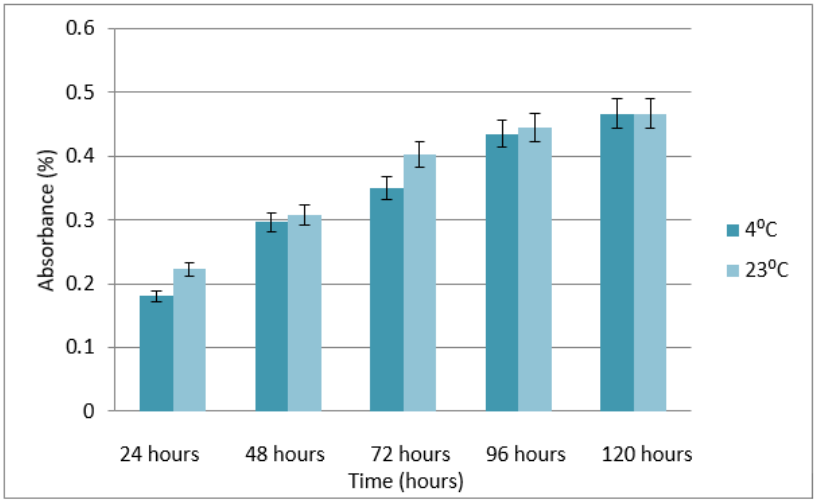

Figure 9. Absorption in saline solution of the PLA sample at temperatures of 4 and 23 ºC, for a storage period of 120 hours

The maximum absorption value of 0.47% is relatively low. In pure water, PLA typically absorbs slightly more water, typically between 0.5% and 1%, depending on its degree of crystallinity. The presence of 10% NaCl in the external solution induces an osmotic effect. The high external salt concentration retains water, reducing its chemical potential and, consequently, the driving force for water ingress into the hydrophobic PLA sample. Therefore, temperature (23ºC versus 4ºC) influences only the rate of equilibrium attainment during the initial days, accelerating the process. The maximum absorption capacity at saturation remains independent of temperature over the 4–23ºC range, limited to 0.47% by the polymer's structural properties and the osmotic pressure exerted by the 10% saline solution.

Goniometric study of a PLA-based sample. Figure 10 shows the sample image together with the contact angle report for the distilled water drop.

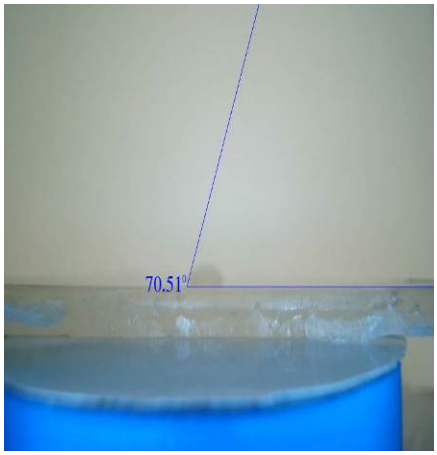

Figure 10. Image of a drop of distilled water deposited on the PLA-ZnO composite

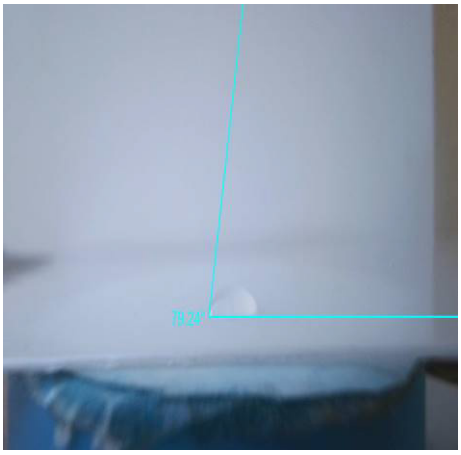

Figure 11. Image of a drop of distilled water deposited on the PLA sample

The PLA-ZnO composite exhibits moderate hydrophilicity, as evidenced by a contact angle of 70.51° between a distilled water droplet and the substrate. This measurement reflects strong water affinity and partial wetting, in contrast to the near-spherical droplets observed on highly hydrophobic materials such as Teflon or wax. In comparison, pure PLA displays a contact angle of 79.24°, which positions it at the threshold between weakly hydrophilic and hydrophobic behavior due to its aliphatic chain structure (Figure 11). The enhanced hydrophilicity of the PLA-ZnO composite, as indicated by its lower contact angle, is attributed to the characteristics of the primary plasticizer (Proviplast 2624) and the specific composite preparation method. During melt processing, Proviplast molecules are likely to orient their polar sides toward the sample surface, particularly when the composite melt remains in extended contact with highly polar metal pressing plates.

The 70.51° contact angle measured for the PLA-ZnO formulation is consistent with the behavior observed in the preceding saline solution test. Although the surface permits water adhesion and wetting, which initiates diffusion, the overall mass absorption remains low at 0.47%.

The incorporation of 3% ZnO into the PLA matrix can alter the contact angle; however, the resulting change in hydrophilicity is not necessarily

linear. This effect depends on the dispersion state of the particles and modifications to surface topography. Zinc oxide is inherently hydrophilic, with numerous polar hydroxyl (−OH) groups present on the particle surfaces. When well dispersed and exposed at the composite surface, these particles increase the material's surface energy, attracting water to the polar centers and reducing the contact angle below 70°. Nevertheless, at a 3% concentration, which represents a critical threshold in composite rheology, ZnO submicron particles tend to agglomerate, unlike the uniform dispersion observed at lower concentrations (0.5 %...1 %). These findings indicate that surface properties differ from bulk properties. While the surface readily interacts with water (contact angle of 70.51°), the compact, predominantly polyester internal structure of PLA restricts deeper water penetration, particularly under the osmotic influence of salt.

Water vapor permeability. The calculation of water vapor permeability was carried out with the relationship (1):

$$WVP = \frac{\Delta M \cdot d}{\Delta t \cdot \Delta P \cdot A}, \quad g \times mm / m^2 \times h \times kPa \tag{1}$$

where:

- ΔM - the difference in weight of the Petri dish before and after the determination, (g)
- Δt – time unit (h),
- d - probe thickness (mm),
- A - the area of the probe exposed to moisture (m^2),
- Δp - the difference in water vapor pressure between the inside and outside of the Petri dish (3.1671 kPa at 25 °C).

The average value of water vapor permeability after three determinations was: WVP = 0.54 $g \times mm / m^2 \times h \times kPa$

FTIR analysis. Figure 12 shows the ATR - FTIR spectrum of the PLA, Proviplast 2624, and ZnO composite. Absorption bands were detected at wavenumbers of 2992, 1747, 1454, 1361, 1267, 1180, 1079, 1043, 956, 865, and 754 cm^{-1}. The peaks at 1747, 1180, and 1079 cm^{-1} exhibit the highest intensities. These last peaks correspond to C–O or C=O stretching, functional groups originated from PLA or plasticizer.

The ATR - FTIR spectrum reveals the predominant features of the polymer matrix (PLA), the effects of the plasticizer, and the specific interactions with the inorganic phase (ZnO). Most of the absorption bands are characteristic of PLA's chemical structure, like 2992 cm^{-1}, specific for C–H

stretching form PLA backbone, or 1454 cm^{-1}, specific for CH_3 asymmetric deformation. The most intense bands confirm the presence of ester groups. The absorption at 1747 cm^{-1} exhibits the highest intensity and corresponds to the stretching vibration of the carbonyl group in the ester bond of PLA, a position typical for amorphous or semi-crystalline PLA. The bands at 1180 cm^{-1} and 1079 cm^{-1} correspond to the asymmetric and symmetric stretching vibrations of the ester bond, respectively, and their high intensities are typical of polyesters. The absorption at 2992 cm^{-1} is attributed to the asymmetric stretching vibrations of methyl groups, while the bands at 1454 cm^{-1} and 1361 cm^{-1} correspond to the deformation vibrations of the $-CH_3$ and $-CH-$ groups. The band at 1267 cm^{-1} is assigned to the stretching vibration of the C−O bond in ether or ester groups [19].

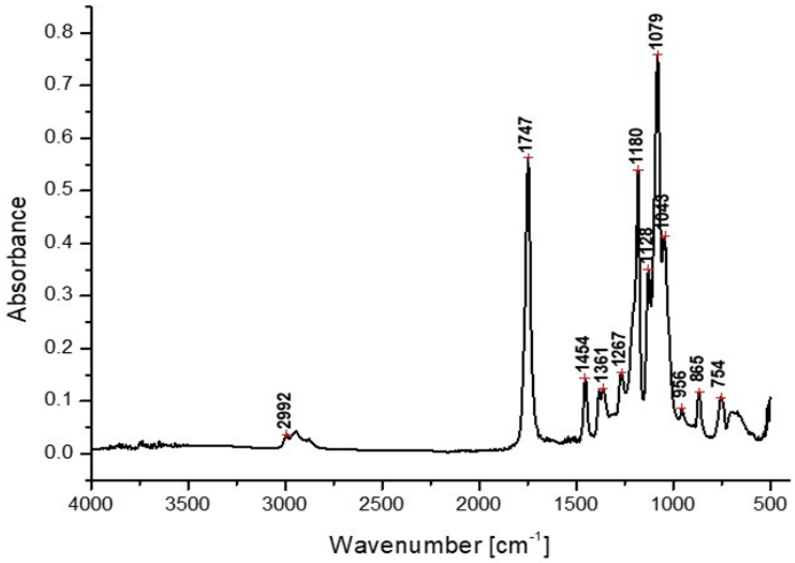

Figure 12. ATR - FTIR spectrum of the PLA – ZnO composite

Also, Proviplast 2624 is an ester-type plasticizer having a chemical structure similar to that of PLA (both contain ester groups), so that its bands overlap those of the polymer. Thus, the presence of the plasticizer can broaden the peak at 1747 cm^{-1}, since it also contains C=O groups, and the 1043 cm^{-1} and 956 cm^{-1} bands are more pronounced due to the specific structure of the plasticizer (vibrations of aliphatic or C−O chains specific to low molecular weight esters).

Zinc oxide, as an inorganic material, exhibits fundamental vibrations typically below 500 cm^{-1} (Zn−O bond), which are not detected in the IR range. Its presence in the composite is inferred from the formation of hydrogen bonds or electrostatic interactions between the ZnO particle surfaces and the polar groups of the polymer or plasticizer, as evidenced by the C=O band at 1747 cm^{-1} and the C−O bands at 1180 cm^{-1}. The high intensities of the bands at 1747, 1180, and 1079 cm^{-1} suggest a structure dominated by ester bonds, confirming effective homogenization of the plasticizer within the PLA matrix and the absence of significant chemical degradation of the polymer during processing. For example, hydrolysis would have produced a broad −OH peak above 3200 cm^{-1}. $^{-1}$. As Kim and co. shows that the presence of plasticizer may increase absorption in the area 1730–1750 cm^{-1}, adding ester carbonyls and slightly shifting the existing peaks [19].

Microbiological analysis

Preparation of Petri dishes and microbial inoculation procedure. For the testing procedure, 15 Petri dishes were used for each condition, containing 15 mL of a culture medium specific for bacterial growth, and an additional 15 Petri dishes containing 15 mL of a culture medium specific for fungal growth. The chemical composition of the culture media is presented in Table 7. The microbial strains *Bacillus subtilis* and *Aspergillus sp.* were obtained from the microorganism collection of the TPP laboratory within UPG. The culture media for bacterial and fungal growth were prepared in accordance with the protocol described in the USP and EU *Pharmacopoeia* [20,22,24].

The sterilized culture media, cooled to 30°C, were poured into labeled Petri dishes. In each Petri dish containing bacterial growth medium, 400 µL of pure *Bacillus subtilis* culture at a concentration of 10^5 cells/mL was added. The media were homogenized by gentle swirling of the plates and allowed to cool at room temperature until solidification.The same procedure was applied to 15 Petri dishes containing fungal growth medium. Each plate was inoculated with 400 µL of pure *Aspergillus* sp. culture at a cell concentration of 10^4 cells/mL.

Table 7. Composition of culture media used in microbiological analyses

Culture medium	Composition	Preparation method
Bacterial growth medium	Peptone 10 g Sodium chloride 5 g Agar 20 g Meat extract 10 g Water up to 1000 mL	The mixture was heated to boiling, the pH was adjusted to 7.4, then filtered and sterilized at 121 °C for 15 minutes
Fungal growth medium	Peptone 10 g Glucose monohydrate 20 g Agar 20 g Water up to 1000 mL	All components were mixed until dissolved, the pH was adjusted to 5.5, and the medium was sterilized at 121 °C for 15 minutes

Assessment of the inhibitory effect of the chemical composition of the tested samples. In each Petri dish, two specimens from Series A (PLA–ZnO CONTROL samples), Series B (inoculated PLA–ZnO samples), and Series C (agar-only film samples) were placed at equal distances from one another on the surface of the culture medium.The Petri dishes inoculated with *Bacillus subtilis* were incubated at 37°C for 48 hours, while those inoculated with *Aspergillus* sp. were incubated at 28 °C for 14 days. After incubation, the bacterial culture plates were examined microscopically. The obtained results were quantified by measuring the zone of microbial growth inhibition according to the protocol described in the USP and EU *Pharmacopoeia* [20,22,24].

Experimental results. The inhibition zones formed around the PLA–ZnO composite samples labeled CONTROL (A1 and A2), compared with the controlled-inoculated PLA–ZnO samples (B1 and B2) and the agar film samples (C1 and C2), were different. As shown in Figure 13, the control samples exhibited the largest inhibition zones. The samples previously contaminated with bacteria showed a smaller inhibition zone. However, it can still be observed that the chemical composition of the PLA exhibits bactericidal potential, considering that the samples were pre-inoculated with microorganisms. Regarding sample C, it was observed that its chemical composition does not exhibit antimicrobial activity, as no inhibition zone was detected. On the contrary, *Bacillus subtilis* was able to grow, since the culture medium was favorable for cellular development. Similar results were obtained in the case of incubation with the fungal strain *Aspergillus* sp.

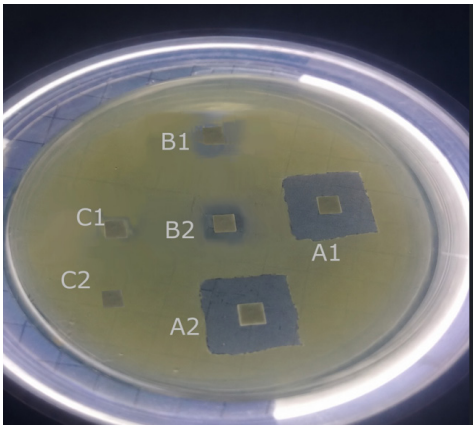

Figure 13. Microscope image of the Petri appearance of Petri dishes inoculated with *Bacillus subtilis* **i**n culture medium after 48 h incubation at 37 °C

Figure 13 illustrates the culture media after incubation, showing the visual appearance of the Petri dishes inoculated with *Bacillus subtilis* and the corresponding samples.

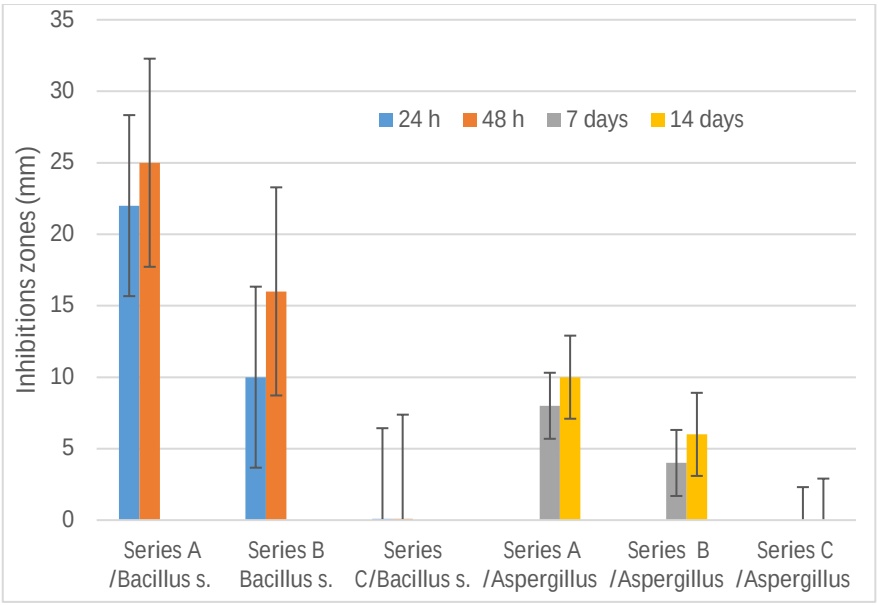

Figure 14. Graphical representation of the experimental results obtained from microbiological tests

Given the results obtained after 48 hours of incubation, which showed a significantly larger inhibition zone than the other samples, the experiment was extended to 72 hours to highlight the microbicidal effect of the ZnO powder within the composite's chemical composition. Thus, larger PLA–ZnO Control samples (50 mm × 50 mm) were transferred onto Petri dishes previously inoculated with *Bacillus subtilis* and containing a culture medium specific for bacterial growth. The results obtained after 72 hours of incubation clearly demonstrated that the inhibition zone generated by the ZnO particle pellets effectively suppressed bacterial growth, maintaining the microorganisms at a distance over time. Figure 14 shows the graphical representation of the experimental results from microbiological tests regarding the inhibition generated by the chemical composition of the analyzed samples. The values are presented as mean ± standard deviation, n = 4, performed in quintuplicate.

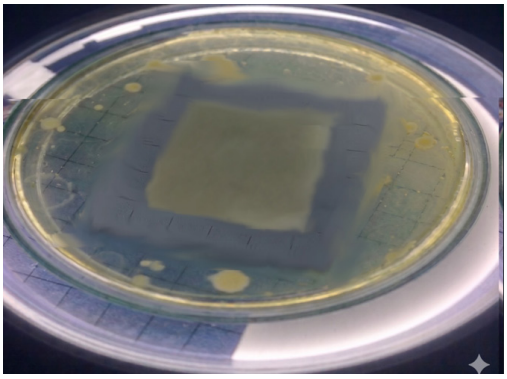

Figure 15. Visual appearance of Petri dishes inoculated with *Bacillus subtilis* in culture medium after 72 h incubation at 37 °C

In addition, the results obtained after 72 hours of incubation showed that bacterial colony-forming units (CFUs) appeared on the Petri dish outside the diffusion zone of ZnO, while inhibition of cellular growth was maintained around the CONTROL sample.

CONCLUSIONS

ZnO powder produced by the precipitation method features a mesoporous structure, partially agglomerated particles, moderate porosity, and a specific surface area suitable for antimicrobial applications. Conducting the precipitation process at a controlled flow rate with 2% wt Polysorbate 80,

followed by 30 minutes of maturation and calcination at 300°C, yields a ZnO powder with a narrow particle size distribution and aggregate-containing ZnO powder with a broad size distribution suitable for antimicrobial applications. The PLA composite containing ZnO demonstrates good mechanical performance, with adequate resistance to bending and tensile stresses. At -18°C, the material supports higher loads than at 4°C, indicating increased strength and stiffness at lower temperatures. However, its relatively low elongation suggests limited flexibility, making it more suitable for applications requiring mechanical stability and rigidity rather than high deformability. The addition of 15% by weight Proviplast 2624 increases PLA chain mobility, which partially reduces the barrier effect of ZnO and allows limited oxygen diffusion through the PLA-based membrane. The measured water vapor permeability indicates good particle dispersion, low porosity, a homogeneous interface, and a structure suitable for packaging or antimicrobial membrane applications. The contact angle of the water droplet with the surface of the PLA-ZnO composite of 70.51° shows a decrease in the hydrophobic character of the composite in the vicinity of the PLA-ZnO composite surface, probably due to the migration of ZnO particles to the composite surface or the orientation of the polar groups of Proviplast 2624 to its surface during the composite preparation process. This contact angle value is consistent with the variation of the absorption of saline water in the composite with the contact time with the saline solution. Microbiological tests have highlighted the important contribution of ZnO particles in inhibiting the growth of *Bacillus subtilis* and *Aspergillus sp*. cultures.

EXPERIMENTAL SECTION

Materials and Methods

For the preparation of ZnO powder, zinc acetate, sodium hydroxide, ethanol, and Polysorbate 80 (Sigma-Aldrich) were used. Zinc oxide was synthesized by precipitation of a 0.1M solution of zinc acetate with a 0.1M solution of NaOH at a flow rate of 0.5 mL/min, in the presence of Polysorbate 80 at a concentration of 2%wt. The reaction was carried out at 60°C in an Erlenmeyer flask equipped with magnetic stirring at 600 rpm to a final pH of 10. The precipitate obtained was washed with distilled water 3 times and then with ethanol, after which it was dried in an oven with air recirculation at 90°C for 3 hours, then calcined at 300°C for 4 hours with a heating rate of 10°C/min. The experimental program was developed in accordance with findings from previous research [22-28].

Biodegradable composite was prepared using PLA (Ingeo® brand, NatureWorks LLC, Tokyo, Japan), plasticizers Proviplast 2624 (Proviron, Hangzhou, China) and Span 60 (sorbitan monostearate, Sabo), and ZnO powder with submicron particles synthesized as described above. The material was produced by hot mixing of components in a Brabender plastograph at 180°C and 60 rpm for 30 minutes, followed by pressing the resulting mixture between hot plates at 170°C for 5 minutes at 100 bar pressure. The formulation consisted of 80% by weight PLA, 15% Proviplast 2624, 2% Span 60 and 3% ZnO powder with submicron particles.

Characterization methods

Characterization of ZnO powder

Characterization of ZnO powder involved determining particle size distribution, textural properties and SEM analysis. Particle size and distribution were measured using a Nano ZS (Red badge) device, calibrated for particle sizes ranging from 0.6 nm to 6 µm, employing the DLS method. The Zetasizer Nano device measures fluctuations in the intensity of scattered light to calculate particle size within the sample.

The textural properties of the samples were evaluated using a Quantachrome NOVA 2200e gas sorption analyzer. Nitrogen adsorption/desorption isotherms were recorded at 77.35 K over a relative pressure (p/p_0) range from 0.005 to 1.0. The total pore volume was estimated from the desorbed volume at a relative pressure close to unity using the BJH (Barrett–Joyner–Halenda) method and the specific surface area was calculated using the BET method.

The structure and morphology of the ZnO powder and the PLA-ZnO composite were analyzed using scanning electron microscopy (SEM-Inspect S, FEI Company) operated at 15 kV.

Characterization of PLA composite

The PLA composite was characterized by measuring flexural and tensile strengths, assessing oxygen and moisture barrier properties, SEM and conducting FTIR analysis.

Mechanical Properties. Mechanical properties were evaluated using a Lloyd LR5k Plus universal testing machine (Lloyd Instruments, AMETEK Inc., West Sussex, UK; 5 kN load capacity) equipped with Nexygen software (version 4.0). All tests were performed at a crosshead speed of 1 mm/min, and each measurement was carried out on ten specimens (n = 10). Results

are reported as mean ± standard deviation. Statistical differences between samples stored at 4 °C and −18 °C were assessed using Student's t-test, with significance set at $p < 0.05$.

Tensile properties were determined according to ISO 527-3:2018 [24,28] using rectangular specimens (40 × 4 × 3 mm). Tensile strength, elongation at break, maximum load, breaking load, and Young's modulus were calculated from the stress–strain curves.

Flexural properties were measured according to ASTM D790 using the three-point bending method [25,30-31] on rectangular specimens (30 × 2 × 2 mm) with a support span of 20 mm. Maximum load, flexural modulus, bending stiffness, maximum flexural stress, and elongation were determined from the load–displacement curves.

Barrier properties. The barrier properties of the PLA were evaluated by measuring oxygen permeability, water absorption, and hydrophobicity using goniometric analysis [32-36].

Oxygen permeability. The determination of oxygen permeability was performed using the manometric method adapted for plastics on a Gaze-LYSSY permeability measuring device, in accordance with ASTM D1434 and ISO 2556, at 1 atm, 23 °C, and 0% relative humidity.

Water absorption. The sample was maintained in a desiccator until a constant weight was achieved, which was recorded as the initial mass (M_initial). The sample was then immersed in 15 mL of 10% saline solution and stored at 4 °C for 24 hours. Prior to weighing, the sample was rinsed with distilled water cooled to 4 °C, blotted with absorbent paper, and weighed three times in quick succession. The resulting value was recorded as the final mass (M_final) for that day. After each weighing, the sample was returned to the bottle, maintained at room temperature (22–23 °C) for 4 hours. The aforementioned steps were then repeated. After each measurement, the sample was returned to the bottle and refrigerated for another 24 hours. This procedure was conducted daily for 7 days. An identical protocol was followed at 23 °C. Absorption was calculated using the formula (2):

$$Ab = \frac{M_{final} - M_{initial}}{M_{initial}} \cdot 100, \quad \% \tag{2}$$

where $M_{initial}$ and M_{final} represent the mass weighed daily at 4° and 23°C, respectively.

Wetting degree by goniometry. A goniometric analysis of the PLA-based sample was performed using a camera connected to a computer running

specialized software. The wetting properties were quantified by measuring the contact angle between a water droplet and the sample surface.

Study of barrier properties. Water vapor permeability was measured using the ASTM E96 gravimetric method. A total of 20 g of anhydrous calcium chloride was placed in a Petri dish, sealed with PLA-based foil, and the assembly was weighed. The assembly was subsequently placed in a desiccator containing 300 ml of distilled water and maintained in an oven at 25°C.

FTIR spectroscopy. The Fourier-transformed infrared (FT-IR) spectra were recorded with a Jasco FTIR spectrometer (Jasco Europe srl, Cremella, Italy), using the total attenuated reflectance (ATR) device equipped with a horizontal ZnSe crystal (Jasco PRO400S, Jasco Inc., Easton, USA). FTIR spectra were registered for all samples at a resolution of 4 cm^{-1} as the mean of 100 scans in the wavenumber range of 4000-500 cm^{-1}.

Microbiological analysis. To evaluate whether the PLA containing ZnO exhibits antibacterial and/or antifungal properties, tests were performed to assess the degree of inhibition generated by the chemical composition of the PLA–ZnO composite in comparison with a plain agar-based sample [10-16]. The analysis procedure was carried out according to the protocol described in the USP and EU *Pharmacopoeia* [20,22,24].

Preparation of test samples. Test specimens were cut into 5 × 5 mm squares from three type materials, as follows: A) PLA–ZnO composite samples labeled CONTROL (Series A); B) PLA–ZnO composite samples subjected to controlled microbial inoculation (Series B); and C) samples cut from an agar film that did not contain any active substances in its composition (Series C).

Procedure for contamination of samples (Series B). The inoculation procedure of the microbial flora onto the surface of the composite PLA–ZnO sample (50 × 50 mm) was performed through controlled contamination using a defined amount of test microorganisms prepared in tenfold serial dilutions in physiological saline. The inoculum was applied onto the sample surface using a micropipette (400 µL of pure culture prepared in serial dilutions: *Bacillus subtilis* at concentrations of 10^5 cells/mL and 10^4 cells/mL, as well as *Aspergillus* sp.). After inoculation, the samples were kept in contact for 10 minutes, during which the inoculated suspension was evenly distributed by gently rotating and spreading it over the sample surface until complete drying at room temperature [25, 27, 29, 37, 38].

ACKNOWLEDGMENTS

Development of innovative food packaging without negative impact on the environment (AMBAL-INOV)", My SMIS: 120994, contract: 375/ 390051/ 30.09.2021, Competition: 63/POC/163/1/3/LDR.

G.V. acknowledges the support of the PN 23.06 Core Program – ChemNewDeal, within the National Plan for Research, Development and Innovation 2022–2027, developed with the support of the Ministry of Research, Innovation and Digitalization, Project No. PN 23.06.02.01, InteGral.

REFERENCES

1. J. Yu; H. Tian; Y. Zhao; L. Li; H. Pan; H. Yang; J. Bian; Z. Tan; H. Zhang. Development of antibacterial PLA-based melt-blown nonwovens via incorporation of P(3HB-co-4HB) and ZnO nanoparticles: Processing and property evaluation. *ACS Appl. Polym. Mater.* **2025**, *7* (18), 12269-12282.
2. C. A. Avila-Orta; C. A. Covarrubias-Gordillo; H. A. Fonseca-Florido; L. Melo-Lopez; R. Radillo-Ruiz; E. Gutierrez-Montiel. PLA/modified-starch blends and their application for the fabrication of non-woven fabrics by melt-blowing. *Carbohydr. Polym.* **2023**, *316*, 120975.
3. Q. Ren; M. Wu; L. Wang; W. Zheng; Y. Hikima; T. Semba; M. Ohshima. Cellulose nanofiber reinforced poly(lactic acid) with enhanced rheology, crystallization and foaming ability. *Carbohydr. Polym.* **2022**, *286*, 119320.
4. D. Li; F. Chen; Z. Dong; F. Jia; R. Wen; C. Sun; Q. Yu. Electrospun PLA/ZnO composite films: Enhanced antibacterial properties and application in fresh chicken meat preservation. *Food Packag. Shelf Life* **2025**, *49*, 101536.
5. A. Torche; T. Chouana; S. A. Uzun; C. A. Isik; M. E. Parlak; M. D'Elia; L. Rastrelli; F. T. Saricaoglu. Biodegradable PLA films plasticized with hydrophobic deep eutectic solvents and enriched with green-synthesized ZnO nanoparticles from date palm pits for antimicrobial food packaging. *LWT* **2026**, *241*, 119105. https://doi.org/10.1016/j.lwt.2026.119105
6. R. Thandavamoorthy; V. Mohanavel; A. Sivapragasam; V. Vekariya; D. Paul; P. Velmurugan; S. Al Obaid; S. A. Alharbi; N. Basavegowda. Environmental sustainability and waste conversion of Prosopis juliflora fibre-reinforced ZnO nanofiller particulates PLA composite - mechanical and thermal analysis. *Heliyon* **2024**, *10* (19), e38327. https://doi.org/10.1016/j.heliyon.2024.e38327
7. J. Chen; R. Tan; J. Ren; M. Huang; L. Wang; Q. Zhang. Polylactic acid (PLA) composites reinforced by end-capped ZnO quantum dots for enhanced mechanical, thermal, and degradation properties. *Polymer* **2025**, *337*, 129007.
8. X. Feng; Y. Guo; N. Zhao; Q. Dong; Z. Li. Bioinspired medical indwelling catheters with hierarchically structured coatings exhibiting specific wettability and antibacterial property. *Colloids Surf. B Biointerfaces* **2023**, *227*, 113388.

9. K. Yang; J. Shi; L. Wang; Y. Chen; C. Liang; L. Yang; L.-N. Wang. Bacterial anti-adhesion surface design: surface patterning, roughness and wettability: a review. *J. Mater. Sci. Technol.* **2022**, *99*, 82-100.
10. M. Carbureanu; C. G. Gheorghe. A machine learning-based data-driven model for predicting wastewater quality parameters in the industrial domain. *Appl. Sci.* **2026**, *16* (2), 694. https://doi.org/10.3390/app16020694
11. R. M. Goulter; I. R. Gentle; G. A. Dykes. Issues in determining factors influencing bacterial attachment: a review using the attachment of Escherichia coli to abiotic surfaces as an example. *Lett. Appl. Microbiol.* **2009**, *49*, 1-7.
12. C. G. Gheorghe; O. Pantea; V. Matei; D. Bombos; A.-F. Borcea. The efficiency of flocculants in biological treatment with activated sludge. *Rev. Chim.* **2011**, *62* (10), 1023-1026.
13. M. Morgelin. *Bacterial Pathogenesis: Methods and Protocols*; P. Nordenfelt; M. Collin, Eds.; Springer: New York, NY, **2017**; pp. 211-217.
14. S. V. Oopath; A. Baji; M. Abtahi; T. Q. Luu; K. Vasilev; V. K. Truong. Nature-inspired biomimetic surfaces for controlling bacterial attachment and biofilm development. *Adv. Mater. Interfaces* **2022**, *10* (4), 2201425.
15. C. McGoverin; C. Steed; A. Esan; J. Robertson; S. Swift; F. Vanholsbeeck. Optical methods for bacterial detection and characterization. *APL Photon.* **2021**, *6*, 080903. https://doi.org/10.1063/5.0057787
16. C. G. Gheorghe; O. Pantea; V. Matei; D. Bombos; A.-F. Borcea. Testing the behavior of pure bacterial suspension (*Bacillus subtilis, Pseudomonas aeruginosa* and *Micrococcus luteus*) in case of hydrocarbons contaminators. *Rev. Chim.* **2011**, *62* (9), 926-929. ISSN 0034-7752.
17. F. Pantanella; P. Valenti; T. Natalizi; D. Passeri; F. Berlutti. Analytical techniques to study microbial biofilm on abiotic surfaces: pros and cons of the main techniques currently in use. *Ann. Ig.* **2013**, *25*, 31-42.
18. T. R. Putri; A. Adhitasari; V. Paramita; M. E. Yulianto; H. D. Ariyanto. Effect of different starch on the characteristics of edible film as functional packaging in fresh meat or meat products: A review. *Mater. Today Proc.* **2023**, *87*, 192-199.
19. K. Tyagi; A. Malik. Antimicrobial action of essential oil vapours and negative air ions against Pseudomonas fluorescens. *Int. J. Food Microbiol.* **2010**, *143* (3), 205-210. https://doi.org/10.1016/j.ijfoodmicro.2010.08.023
20. Chapter 2.6.12, 2.6.13. Microbiological Examination of Non-sterile Products-Microbial Enumeration Tests, *European Pharmacopoeia*, **2013** Edition. Available online: https://ehpm.org/wp-content/uploads/2022/04/QG22_2-6-12_Microbiological_examination_of_non-sterile_products-microbial_enumeration_tests_ep10-2.pdf
21. J. K. Nayak, L. Behera, B. R. Jali. TiO_2 strengthened PLA nanocomposites: A prospective material for packaging application, *J. Mol. Struct.,* **2024**, *1316*, 138892, https://doi.org/10.1016/j.molstruc.2024.138892
22. NCCLS Performance Standards for Antimicrobial Disk and Dilution Susceptibility Tests for Bacteria Isolated from Animals, Approved Standard. 2nd Edition, NCCLS Document M31-A2 22(6), *Clinical and Laboratory Standards Institute,* Wayne, **2002** Available online: https://www.dbt.univr.it/documenti/OccorrenzaIns/matdid/matdid485539.pdf

23. C. G. Gheorghe; C. Dusescu; M. Carbureanu. *Asphaltenes biodegradation in biosystems adapted on selective media*. Rev. Chim. **2016**, *67* (10), 2106-2110.
24. Microbiological Examination of Non-Sterile Products: Microbial Enumeration Tests <61>; USP 39-NF 34; *United States Pharmacopeial Convention*: Rockville, MD, USA, **2016**; Available online: https://www.usp.org/sites/default/files/usp/document/harmonization/gen-method/q05b_pf_ira_34_6_2008.pdf
25. D. R. Popovici; C. G. Gheorghe; C. M. Dusescu-Vasile. Assessment of the active sludge microorganisms population during wastewater treatment in a micro-pilot plant. *Bioengineering* **2024**, *11* (12), 1306.
26. Japanese Industrial Standards Association. *JIS Z 2801:2010 Antibacterial Products - Test for Antibacterial Activity and Efficacy*; Japanese Industrial Standards Committee: Tokyo, Japan, **2010**.
27. C. G. Gheorghe; O. Pantea; V. Matei; D. Bombos; A.-F. Borcea. Testing of bacterial and fungal selection in the pollution of water with cationic detergents. *Rev. Chim.* **2011**, *62* (7), 707-711.
28. A. L. Koch. Growth Measurement. In *Methods for General and Molecular Bacteriology*; P. Gerhardt et al., Eds.; American Society for Microbiology: Washington, DC, **1994**; pp. 248-277.
29. F. Lupu; C. G. Gheorghe; C. Calin; O. Pantea. Biotreatment of the oil pollutants. *Rev. Chim.* **2013**, *64* (2), 210-212. ISSN 0034-7752.
30. C. Wiegand; A. Volpel; A. Ewald; M. Remesch; J. Kuever; J. Bauer; et al. Critical physiological factors influencing the outcome of antimicrobial testing according to ISO 22196/JIS Z 2801. *PLoS One* **2018**, *13*, e0194339.
31. P. Gilbert; et al. Inocula for antimicrobial sensitivity testing: a critical review. *J. Antimicrob. Chemother.* **1987**, *20*, 147-154.
32. General Chapter <62> Microbiological Enumeration of Non-Sterile Products - Tests for Specified Microorganisms. *USP 35-NF 30*; United States Pharmacopeial Convention, Inc.: Rockville, MD.
33. R. H. Katzenberger; A. Rosel; R. P. Vonberg. Bacterial survival on inanimate surfaces: a field study. *BMC Res. Notes* **2021**, *14*, 97.
34. S. Maitz; S. Polzl; D. Dreisiebner; C. Kittinger. Antimicrobial non-porous surfaces: a comparison of the standards ISO 22196:2011 and the recently published ISO 7581:2023. *Front. Microbiol.* **2024**.
35. EP. 5.1.3 Efficacy of Antimicrobial Preservation. *Pharm. Eur.* **2006**, *5.0*, 447-449.
36. Validation of Alternative Microbiological Method <1223>. *USP 39-NF 34*; United States Pharmacopeial Convention: Rockville, MD.
37. M. D. Campos; P. C. Zucchi; A. Phung; S. N. Leonard; E. B. Hirsch. The activity of antimicrobial surfaces varies by testing protocol utilized. *PLoS One* **2016**, *11*, e0160728. https://doi.org/10.1371/journal.pone.0160728
38. C. G. Gheorghe; C. M. Dusescu-Vasile; D. R. Popovici; D. Bombos; R.-E. Dragomir; F. M. Dima; M. Bajan; G. I. Vasilievici. Monitoring the biodegradation progress of naphthenic acids in the presence of *Spirulina platensis* algae. *Toxics* **2025**, *13* (5), 368.